Jurnal Tribologi 40 (2024) 39-60

Jurnal Tribologi
Website : jurnaltribologi.mytribos.org
e-issn: 2289-7232

Elastohydrodynamic analysis of composite material with roughness effect on multistep journal bearing tribological performance

Muchammad Muchammad *, Mohammad Tauviqirrahman, Savero Farhansyah, Muhammad Iqbal, Budi Setiyana, J. Jamari

Mechanical Engineering Department, University of Diponegoro, INDONESIA.
*Corresponding author: m_mad5373@yahoo.com

KEYWORDS

Composite Material
Elastohydrodynamic
Multistep Journal Bearing
Numerical Simulation
Roughness

ABSTRACT

Journal bearing is a specific type of bearing in which a lubricating liquid separates the inner surface of the bearing from the contacting shaft. Elastohydrodynamic lubrication modeling is a technique used for modeling journal bearing, taking into account the impact of deformation caused by the pressure generated due to the wedge effect resulting from shaft eccentricity during rotation. In this research, CFD software was used to model textured multistep journal bearing while considering the impact of surface roughness on composite material. According to the simulation results, the effect of multistep texture on the journal bearing increased load carrying capacity at low eccentricity ratios and decreased at high eccentricity ratios, while friction force and acoustic power level reduced as the eccentricity ratios increased. In addition, the effect of composite material on lubrication modeling could be observed in the resulting pressure value. In this context, the higher the elastic modulus of the composite material, the lower the pressure due to deformation. Tribological performance was influenced by roughness levels on the bearing surface and tended to decline as roughness value on the bearing surface increased.

Received 26 July 2023; received in revised form 12 October 2023; accepted 6 November 2023.
To cite this article: Muchammad et al., (2024). Elastohydrodynamic analysis of composite material with roughness effect on multistep journal bearing tribological performance. Jurnal Tribologi 40, pp.39-60.

1.0 INTRODUCTION

Journal bearing is one of the components used in machining systems, and it is a simple bearing model widely used in industry and generating turbines. This type of bearing operates by enclosing the rotating shaft in a cylinder and maintaining separation between the shaft and the bearing surface through the use of lubricating fluid. Subsequently, the performance and durability of journal bearing are influenced by numerous factors Therefore, there is a need to develop research on journal bearing in order to obtain optimal performance. The demand for high-speed machines has dramatically increased in recent years due to the high demand for productive and affordable industrial machinery. This results in an increase in the pressure distribution that occurs in journal bearing. Operating at high speeds, journal bearing exhibits an elevated pressure distribution, resulting in elastic deformation of the bearing surface. The lubrication performance that occurs when journal bearing is operating will be impacted by the elastic deformation that occurs in journal bearing (Lahmar et al., 2010; Muchammad et al. 2022a; Muchammad et al. 2022b).

Pressure fluctuations in journal bearing modeling can lead to cavitation issues, particularly in convergent and divergent zones. Cavitation takes place in the divergent zone, causing a pressure reduction that benefits the convergent region. This phenomenon results in a reduction in the lubricant phase because the lubricant forms a new phase, known as the vapor phase, and the pressure value on journal bearing may decrease as a result of the cavitation event (Dhande & Pande, 2017). Modeling the lubrication of journal bearing encounters challenges due to turbulent flow effects. As the rotor rotational speed increases, the lubrication fluid flow in journal bearing becomes unstable, leading to a transition into turbulent flow (Lin et al., 2018). Compared to plain journal bearing, textured journal bearing have lower friction (Cupilard et al., 2008). The decrease in load-carrying capacity will be impacted by the incorrect form of the texture and arrangement on journal bearing surface (Chen et al., 2020; Tala-Ighil, 2011; Tauviqirrahman et al., 2019). Compared to other textures that enhance lubrication performance within specific eccentricity ratio and rotational speed conditions, a multistep texture model is a straightforward approach for journal bearing texture (Bompos and Nikolakopoulos, 2016; Muchammad et al. 2022b). Subsequently, performance is significantly influenced by the placement and amount of step textures, where the more steps, the less the tribological performance will be (Liang et al., 2016). In order to achieve the best tribology performance, an eccentricity ratio between 0.1 and 0.4 is used (Singh and Awasthi, 2020).

Scientists performed tests on journal bearing material made of metal matrix composite (MMC) and found that this material performed better in terms of wear rate and friction than conventional metal material (Sander et al., 2016). The manufacturing process employed for creating journal bearing includes grinding, which is the technique used to reduce the particle size of a material from a coarser shape to a finer one. This process is used to achieve thorough mixing, ensuring even combination while preventing the segregation of material particles (Groover, 2013). When improving surface texture for journal bearing modeling, surface roughness must be taken into consideration. In general, surface texture and surface roughness play an essential role in optimizing tribological performance of journal bearing (Song et al., 2015). Roughness should be properly considered in deformation situations since it impacts the hydrodynamic outcomes (Javorova, 2016).

Tribological performance of journal bearing is determined through numerical computations due to the development of CFD-FSI coupled methods. In this current research, ANSYS CFD software was used to perform a numerical simulation that focuses on solving the conservation equation of mass, momentum, turbulence, cavitation, load support, friction force, and acoustic

power level. The emphasis is on examining journal bearing lubrication performance influencing composite material with a surface roughness that has not been found in previous studies. Therefore, this research aimed to improve the performance and durability of journal bearing, making them more valuable in the field of machinery.

2.0 METHOD

2.1 Governing Equations

In this research, the Navier-Stokes equation of continuity is used to solve the problem using a numerical technique with steady, incompressible conditions and momentum conservation. The equation is presented as follows (Cupilard et al., 2008):

$$\nabla \cdot \overrightarrow{v} = 0 \tag{1}$$

$$\frac{\partial}{\partial_t}(\rho\vec{v}) + \nabla(\rho\vec{v}\vec{v}) = -\nabla p + \nabla \cdot (\bar{\bar{\tau}}) + \rho\vec{g} \tag{2}$$

Where ρ is the density of the fluid, $\vec{v}$ is the velocity of the fluid, p is the pressure gradient, $\vec{g}$ is gravity, and $\bar{\bar{\tau}}$ is pressure tensor. Pressure tensor is needed for future calculation performance load carrying capacity of the bearing, it defined as follows:

$$\bar{\bar{\tau}} = \mu\left[(\nabla\vec{v} + (\nabla\vec{v})^T) - \frac{2}{3}\nabla \cdot \vec{v}\bar{\bar{I}}\right] \tag{3}$$

In this computation, the RANS (Reynolds Averaged Navier Stokes Simulation) equation is used to account for turbulent phenomenon. This model is selected for its ease of convergence and its ability to address turbulence in various flow configurations. The following is the RANS equation for the determination of the general shape of the inner pressure film for an incompressible viscous fluid.

$$\frac{\partial}{\partial x_j}(\rho u_i u_j) = -\frac{\partial p}{\partial x_i}\left[\mu\left(\frac{\partial u_i}{\partial x_j} + \frac{\partial u_j}{\partial x_i}\right)\right] + \frac{\partial}{\partial x_j}(-\rho u'_i u'_j) \tag{4}$$

Term $-\rho u'_i u'_j$ is known as turbulent component. In this research, turbulence is solved by standard k and ε models. Where k is turbulent kinetic energy and e is the turbulent dissipation rate. Subsequently, lubricant cavitation frequently occurs during journal bearing operation, particularly in the divergent zone. Since cavitation is assumed to be caused by a change in fluid pressure, the cavitation phenomenon in the computational fluid domain is always represented using a phase change boundary condition. In this model, the formation of gas bubbles commonly accompanies the cavitation process. The cavitation and fluid models are coupled through momentum and a single set of density equations for the mixture. The cavitation and fluid models are coupled through momentum and a single set of density equations for the mixture. The validity of this model has been proved in previous investigations. Three cavitation models are available in ANSYS FLUENT®, which are the Schneer and Sauer model, the Zwart-Gelber-Belamri model, and the Sighal et al. model. The Zwart-Gelber-Belamri model is used in this research due to their ability

to converge fast and be less sensitive to mesh density. The liquid-vapor mass transfer in cavitation (evaporation and condensation) is represented by the vapor transport equation:

$$\frac{\partial}{\partial t}(a_v \rho_v) + \nabla \cdot (a_v \rho_v v) = R_g - R_c \tag{5}$$

Where a_v is vapor volume fraction and ρ_v is vapor density. R_g and R_c account for the mass transfer between the liquid and vapor phases in cavitation. The Zwart-Gelber-Belamri model assumes that all the bubbles have the same size in a system, the final form of the cavitation is as follows:

$$p \leq p_v, R_g = F_{evap} \frac{3\alpha_{nuc}(1-\alpha_v)\rho_v}{R_B} \sqrt{\frac{2}{3}\frac{P_v - P}{\rho_l}} \tag{6}$$

$$p \geq p_v, R_c = F_{cond} \frac{3\alpha_v \rho_v}{R_B} \sqrt{\frac{2}{3}\frac{P - P_v}{\rho_l}} \tag{7}$$

Where F_{evap} = evaporation coefficient = 50, F_{cond} = condensation coefficient = 0.01, R_B = bubble radius = 10^{-6} m, α_{nuc} = nucleation site volume fraction = $5\text{x}10^{-4}$, ρ_l = liquid density and p_v = vapor pressure.

The term fluid-structure interaction (FSI) refers to the connection of the computational fluid dynamic (CFD) and finite element method (FEM) software environments. The deformation of the shaft journal and the housing is calculated for the FSI analysis. The balancing equation regulating the solid domain for issues with solid dynamics was derived from Newton's second law reads:

$$\rho_s \ddot{d}_s = \text{div}\, \sigma_s + F_s \tag{8}$$

Where subscript s refers to the solid designation, ρ is the density and denotes the local acceleration vector, σ indicates the stress tensor and F_s expresses the body force vector.

The ANSYS program uses the FLUENT module for solving lubricant performance using the finite volume technique, while mechanical performance of bearing is estimated through FEM in the transient structural module of this version. When using ANSYS, system coupling may enable the execution of data exchange between fluid and solid analysis in accordance with the appropriate iteration stagger.

Surface roughness variations can occur due to post-production polishing of journal bearing. In order to examine the influence of roughness, this research represents the roughness as uniform sand-grain roughness defined by height parameter K_s as shown in Figure 1. This model assumes a constant height for each grain on the surface. The surface boundary condition in ANSYS FLUENT® requires the roughness height K_s to be provided for calculations.

It should be noted that the roughness height K_s is not equal to the geometric roughness height of the surface, rather it is the corresponding sand-grained roughness height. Therefore, it is necessary to link the equivalent sand-grain roughness height with the appropriate geometric roughness parameters as determined by surface roughness parameters, such as R_a (arithmetic average of the roughness profile). The link between K_s and R_a, according to (Adams et al., 2012), may be roughly described as follows:

$$K_s = 5.863\, R_a \tag{9}$$

Since the correlation shown in Eq. (9) has been experimentally proven (Adams et al., 2012), the surface roughness parameter R_a measured by the profilometer may be used as an input to determine the roughness of the bearing surface in all subsequent computations.

2.2 Performance Equation

The entire amount of load that may be carried by the distribution of the film thickness on the bearing is defined as an integral of the distribution profile pressure over the journal bearing area. The equation of Raimondi-Boyd below can be used to mathematically represent the load-carrying capability W of journal bearing (Meng et al., 2016):

$$W = \iint_A p \, dA \tag{10}$$

The frictional force F_f is defined as the integral of the shear stress along the surface of journal bearing. The following equation of Richard Feynman can be used to mathematically represent the frictional force that occurs in journal bearing (Meng et al., 2016):

$$F_f = \iint_A \tau \, dA \tag{11}$$

An acoustic characteristic occurs when the noise is brought on by turbulence in textured journal bearing. The equation of A.G Bell below is used to calculate the CFD package, which uses the acoustic power level L_p to make an analysis (Meng et al., 2016):

$$L_p(dB) = 10 \log\left(\frac{W}{W_{ref}}\right) \tag{12}$$

Where W_{ref} is the referenced acoustic power as the human hearing threshold is assumed to be 10^{-12} W/m^3.

2.3 Method and Validation

This research used Bompos as its model. The variation of the textured geometry that Bompos examined yielded the optimal geometry, which is applied. Figure 1 and Table 1 show three steps distributed along the journal with a particular parameter.

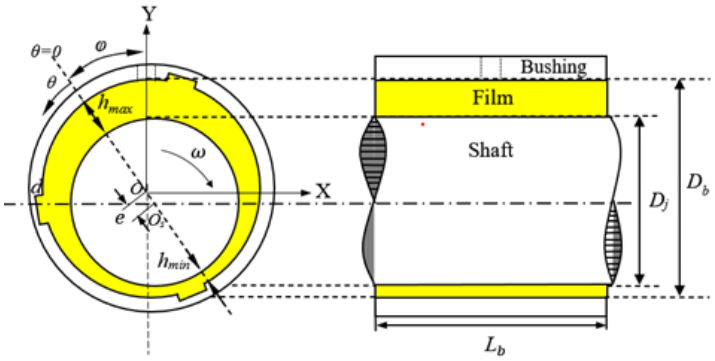

Figure 1: 3D Model of multistep journal bearing.

Table 1: Geometry parameters for multistep journal bearing.

Parameters	**Symbol**	**Value**	**Unit**
Journal radius	R_j	50	mm
Bearing radius	R_b	50.1	mm
Clearance	C	85.5	mm
Eccentricity ratio	ε	0.2; 0.4; 0.6; 0.8	-
Rotational Speed	ω	4,000	RPM
Roughness Levels	R_a	0; 0.1; 0.4;1.6; 6.3	µm
Attitude angle	φ	35	◦
Length-to-diameter ratio	L/D	0.5	-
Step depth	d	0.513	mm
Arc length steps	γ	30	◦
Arc length between steps	β	90	◦
Orientation angle	ψ	5	◦

For further discussion, step *a* is located between 90-120°, step *b* is located between 210-240°, and step *c is* located between 330-360°. The orientation angle is determined after the attitude angle of the journal. This simulation method is based on an investigation by (Dhande & Pande, 2017), which used the SIMPLE method for the Scheme, PRESTO! First-order Upwind is used to calculate pressure; Second-order Upwind is used to calculate density, vapor, energy, and momentum. The next step is to calculate the Under Relaxation Factor (URF) to regulate the simulation-based solution. In order to stabilize and correct the convergence of numerical scheme including iterative operation, URF is used in steady-state flow types in numerical computation. While in theory altering the value of under relaxation factor will not change the outcome of the simulation, it can shorten the time it takes to perform the numerical computation. Therefore, the recommended default value of under relaxation factor is applied in this final project. Table 2 shows additional simulation-related parameters.

Table 2: materials properties parameters for multistep journal bearing.

Parameters	**Symbol**	**Value**	**Unit**
Oil (10W40 SAE)			
Oil liquid density	ρ_o	850	kg/m^3
Oil liquid viscosity	μ_o	0.0125	Pa.s
Oil vapour density	ρ_V	10.95	kg/m^3
Oil vapour viscosity	μ_V	2×10^{-5}	Pa.s
Vapour saturation pressure	P_{sat}	29,185	Pa
Shaft: Steel			
Elastic Modulus	E_S	210	GPa
Density	ρ_S	7,850	kg/m^3
Poisson ratio	υ_S	0.3	-
***Bushing* 1: Aluminum**			
Elastic Modulus	E_A	70	GPa
Density	ρ_A	2,700	kg/m^3
Poisson ratio	υ_A	0.334	-
***Bushing* 2: PMC - GFRP**			
Elastic Modulus	E_A	72.3	GPa
Density	ρ_A	2,580	kg/m^3
Poisson ratio	υ_A	0.3	-
***Bushing* 3: PMC - CFRP**			
Elastic Modulus	E_A	590	GPa
Density	ρ_A	1,900	kg/m^3
Poisson ratio	υ_A	0.3	-
***Bushing 4*: CMC – SiC-SiC**			
Elastic Modulus	E_A	270	GPa
Density	ρ_A	2,600	kg/m^3
Poisson ratio	υ_A	0.3	-
***Bushing 5*: MMC – Al-SiC**			
Elastic Modulus	E_A	220	GPa
Density	ρ_A	3,010	kg/m^3
Poisson ratio	υ_A	0.3	-

A tetrahedral meshing approach with a size of 0.4 mm was used, leading to a total of 82,080 elements and 167,040 nodes, as shown in Figure 2. The result of the meshing in multistep journal bearing simulation model has a maximum skewness of 0.37, which is considered to be good. The largest skewness in plain journal bearing is 0.50, which is considered acceptable.

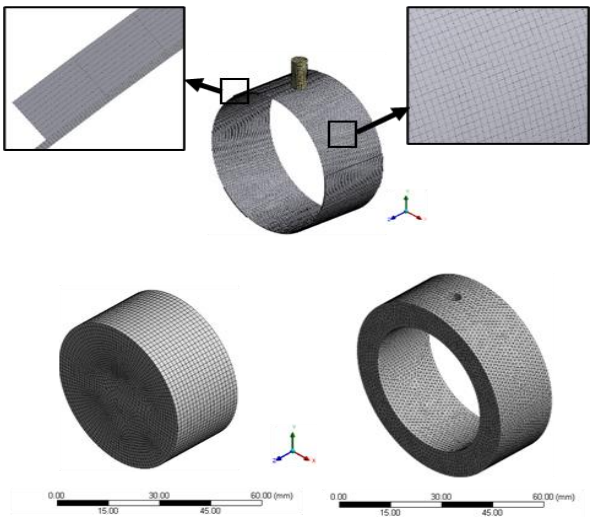

Figure 2: 3D Meshing result for multistep journal bearing.

Figure 3 shows the boundary condition for validation and multistep journal bearing. In this simulation setup, the bearing interface serves as a fixed wall, while the journal interface acts as a moving wall. Both the fixed and moving walls are subject to a no-slip condition. Pressure at the inlet and outflow is assumed to be 0 Pa for validation purposes. Cavitation models use the Zwart-Gelber-Belamri model with the two-phase mixture for the fluid.

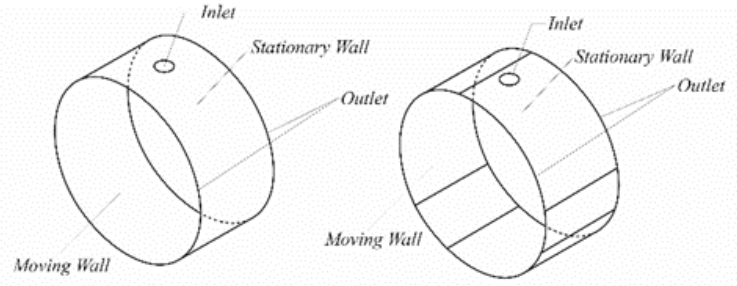

Figure 3: Boundary condition for validation and multistep journal bearing.

It is to emphasize the significance of an independent grid before going into the validation aspect. To reduce computing time, the appropriate level of meshing is determined using grid independence. Figure 4 shows grid independence. Using CFD software, the validity of this research is compared to (Dhande & Pande, 2017). Figure 5 shows the pressure distribution near

the center of the journal with an eccentricity ratio ε = 0.8 and rotation speed ω = 4000 RPM. This validation is successful, as both the maximum pressure and trend fall within a tolerance of 0.15% inaccuracy when compared to the reference. In future simulations, this model can be leveraged to assess the impact of deformation and cavitation.

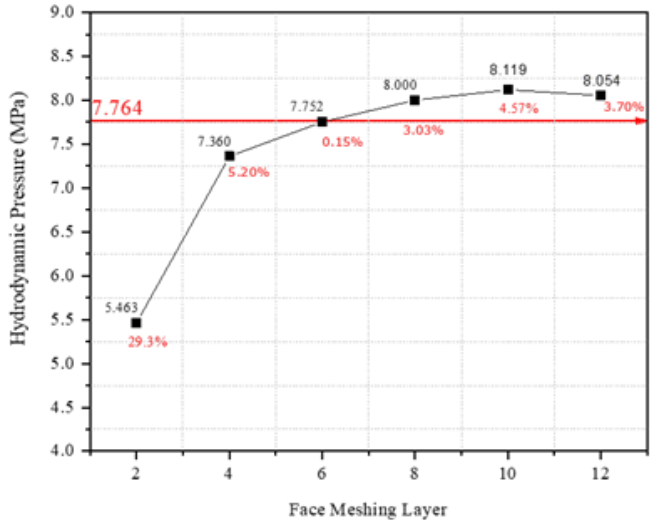

Figure 4: Grid Independency.

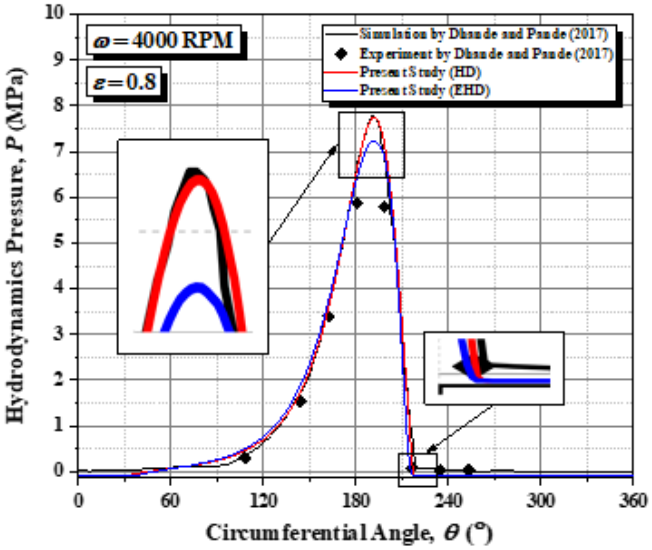

Figure 5: Comparison pressure result from (Dhande et al. 2017) with this present research at mid-plane.

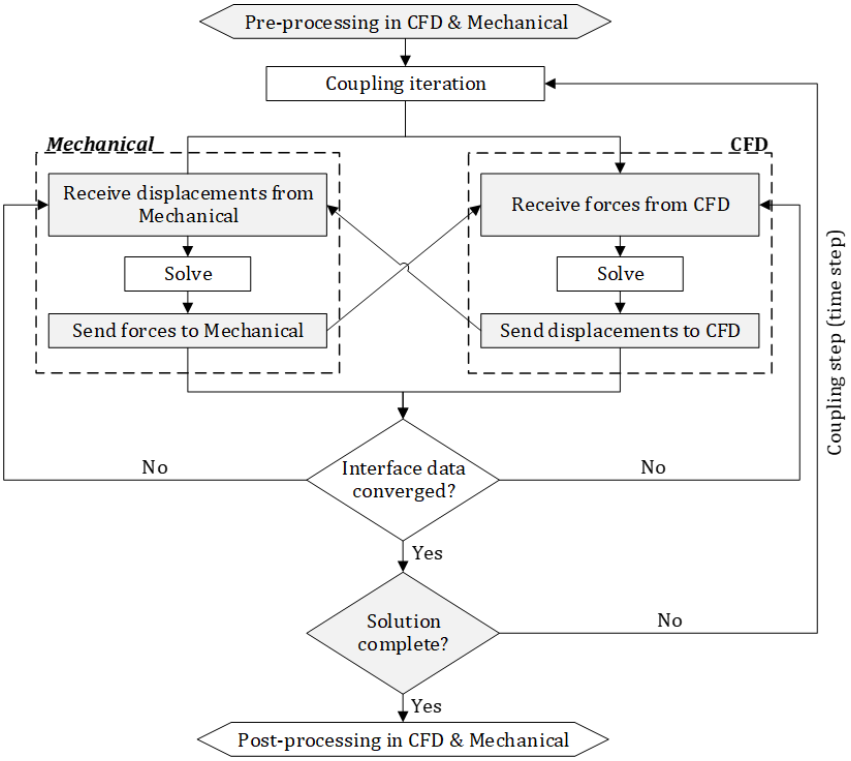

Figure 6: Flow chart process.

Figure 6 shows the process simulation flow of this research using the FSI method, which combines mechanical and CFD iteration. The simulation starts with displacements and forces data from CFD and mechanical results. Furthermore, if the iteration converges, the next step is the solution. If this step is completed, the next step is post-processing. If the iteration fails to converge and the solution is incomplete, the simulation flow is restarted from the combined iteration.

3.0 RESULTS AND DISCUSSION

3.1 Effect of Eccentricity Ratio

In this section, the comparison of tribological performance on each plain and multistep journal bearing eccentricity ratio with a rotation speed of 4000 RPM will be discussed. The focus will be on the assessment of three key aspects of tribological performance, namely load carrying capacity, frictional force, and average acoustic power level of dB.

Figure 7 shows the comparison of pressure distribution between plain and multistep bearing. The greater the eccentricity value, the pressure value will increase and plain condition has a slightly higher value than multistep. The largest value of hydrodynamic pressure is found in plain bearing with an eccentricity ratio of 0.8. The smallest pressure value is found in multistep bearing with an eccentricity ratio of 0.2. The pressure graph shows that the distribution of pressure values varies depending on the current simulation case. Subsequently, it can be seen that plain bearing

case with ε 0.8 has the greatest pressure distribution area from an angle of 80° to 220°. Multistep bearing has the narrowest pressure distribution, ranging from 130° to 220°. This hydrodynamic pressure will have an impact on the bearing load-carrying capacity value. A wider pressure distribution with greater value will produce a greater load-carrying capacity value.

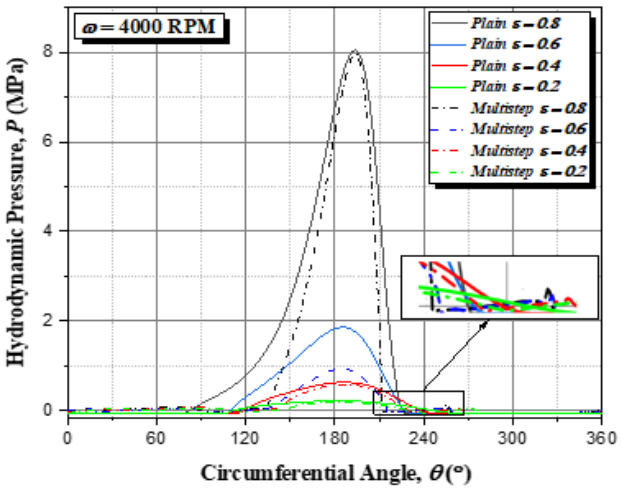

Figure 7: Comparison of the pressure distribution on the angle between plain and multistep journal bearing at various eccentricity ratios.

The eccentricity ratio increases in both plain and multistep journal bearing and the pressure values also increase. However, multistep journal bearing maintains lower pressure values compared to plain journal bearing, and it also has an impact on the value of load-carrying capacity. As shown in Figure 8, the load-carrying capacity of multistep journal bearing is lower than plain journal bearing at all rotational speeds. This is supported by the claim of (Chen et al., 2020) that adding a groove to journal bearing has a significant impact on how well it lubricates, one of the consequences of which is a reduction in load-carrying capability. In addition, the impact of eccentricity ratio on the functionality of tribological journal bearing is a condition that needs to be taken into consideration. As shown in Figure 7, the value of the load-carrying capacity will grow for every increase in the eccentricity ratio. This phenomenon is supported by simulations conducted by (Dhande & Pande, 2017).

Figure 8 shows the comparison of load-carrying capacity between plain and multistep journal bearing. The load-carrying capacity is influenced by the eccentricity ratio, the higher the eccentricity ratio value, the more the load-carrying capacity value. The largest load-carrying capacity value is found in plain bearings with an eccentricity ratio of 0.8. A bearing with an eccentricity ratio of 0.2 produces the load-carrying capacity value. This diagram shows the operation of journal bearing hydrodynamic pressure. When a lubricant crosses a converging gap with a high eccentricity ratio, layer thickness builds up, causing the pressure in the lubricant to increase. This increase in pressure will also increase the force acting on the shaft, allowing it to withstand the load using a parameter known as load-carrying capacity. In journal bearing with a small eccentricity ratio value, the lubricant will experience a minimal increase in the lubricant layer when passing through the convergent gap, resulting in a lower pressure.

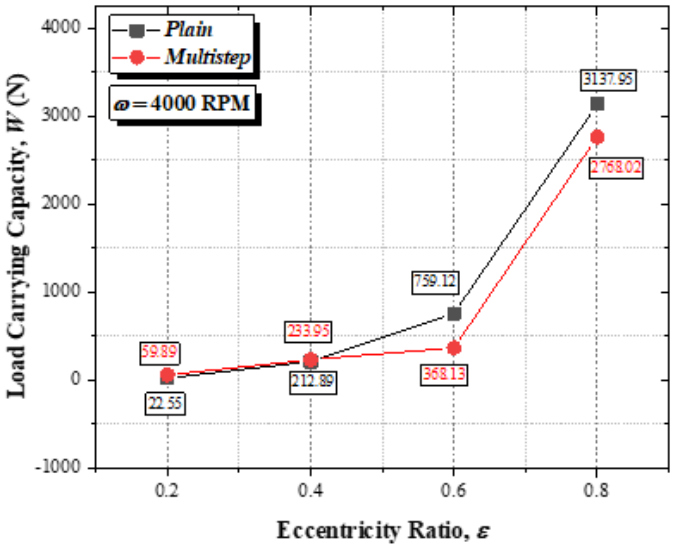

Figure 8: Comparison of the load-carrying capacity of plain and multistep journal bearing at various eccentricity ratios.

Figure 9 shows a comparison of friction forces between plain and multistep journal bearing. Increasing the eccentricity ratio can increase the friction force, but under certain condition, the friction force can decrease, such as at an eccentricity ratio value of 0.6. The highest friction force is observed in plain bearing with an eccentricity ratio of 0.8, while the lowest is in multistep bearing with an eccentricity ratio of 0.6. The graph indicates an interesting feature of the simulation results: increasing the eccentricity ratio value does not always increase the friction force value. The friction force decreases to 4.92 at an eccentricity ratio of 0.6 multistep bearing, while previously an eccentricity ratio of 0.4 produced a value of 10.6 and increased again at an eccentricity ratio of 0.8 with a value of 13.38.

Figure 10 shows the average acoustic power level comparison between two types of journal bearing. The average acoustic power level decreases due to the presence of multistep texturing. This reduction occurs because textured surface reduces turbulent intensity in the textured region, thereby lowering acoustic power levels. The graph shows that increasing the eccentricity ratio value does not always increase the average acoustic power level value. Multistep bearing with an eccentricity ratio of 0.6 has a value of 52.13 dB, while the acoustic level value with an eccentricity ratio of 0.4 previously had a value of 59.51 dB and experienced an increase with an eccentricity ratio of 0.8 with a value of 58.99 dB. One of the causes of changes in values due to the resulting pressure difference, which affects the resulting friction force, is fluid friction with the shaft walls and bearings.

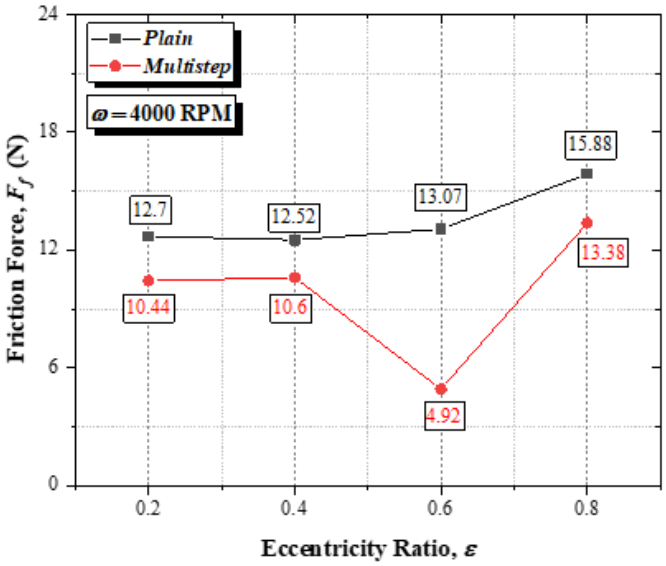

Figure 9: Comparison of plain and multistep friction force values at certain eccentricity ratio conditions.

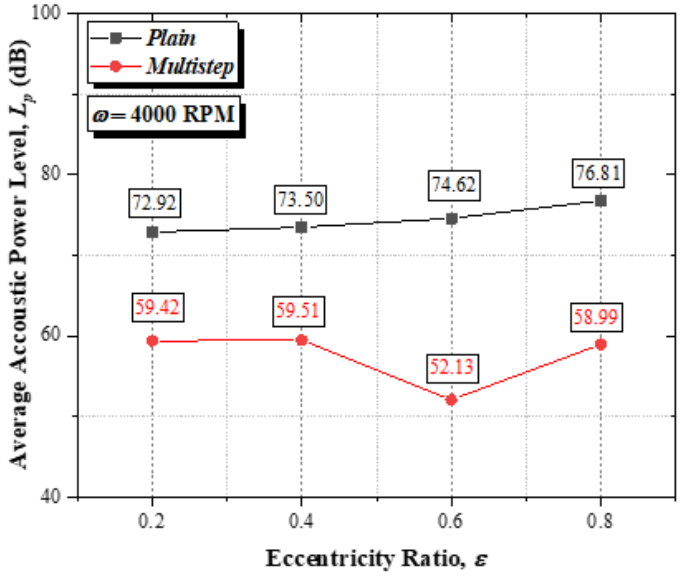

Figure 10: Comparison of the average acoustic power level of plain and multistep journal bearing at various eccentricity ratios.

3.2 Effect of Composite Material

In this section, the performance of elastohydrodynamic lubrication on multistep journal bearing in terms of tribology will be compared with various composite bearing materials. The evaluation will be conducted at an eccentricity ratio of 0.8 and a rotational speed of 4000 RPM,

focusing on key tribological aspects sudh as load carrying capacity, frictional force, and average acoustic power level in dB.

Figure 11 shows that when compared to other composite materials and aluminum, carbon has the highest pressure value. This result can be attributed to the exceptional mechanical characteristics of the carbon fiber-reinforced polymer composite material, which, in comparison to other materials, has a very high elasticity modulus (*E*). Figure 11 also shows that the hydrodynamic pressure will be decreased because of the material modulus of elasticity. Higher modulus will create smaller deformations that will affect the film thickness and have a minor effect on the hydrodynamic pressure. The highest maximum pressure value is found in the CFRP material and the lowest is in the GFRP material. This phenomenon is due to deformation in the material, particularly in convergent gaps, which widens the lubrication area. By expanding the lubrication area, the lubricant will experience fewer fluid particle collisions, reducing the resulting force and potentially affecting the pressure distribution. This pressure will affect the value of the journal-bearing performance in the form of load-carrying capacity.

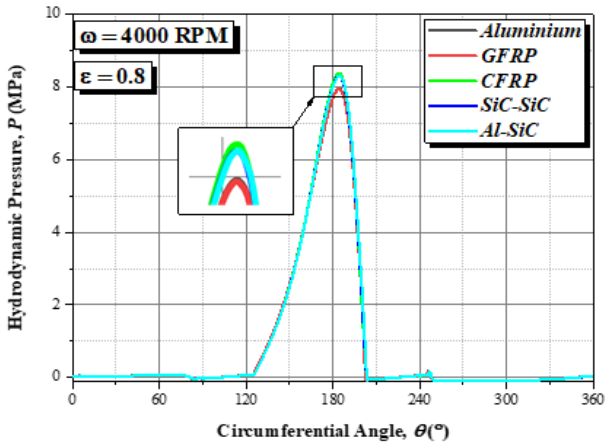

Figure 11: Comparison of the pressure distribution on multistep journal bearing at various bearing materials.

Figure 12 shows the load-carrying capacity is influenced by the hydrodynamic pressure that will be decreased because of the material modulus elasticity. The highest load-carrying capacity value is found in Al-SiC material and the lowest in GFRP material. The material differences can affect the value of the resulting load-carrying capacity, as shown in this graph. The basic factors that influence this value are the type of materials and characteristics. The elastic modulus value is one of the material parameters that influence it. The elastic modulus is significant because it can affect the resulting deformation change value. The greater the resulting deformation value, the more the collision value of flowing fluid particles will change. Subsequently, particle collisions cause changes in force and momentum, which have a large impact on the pressure distribution, causing the load-carrying capacity value to change.

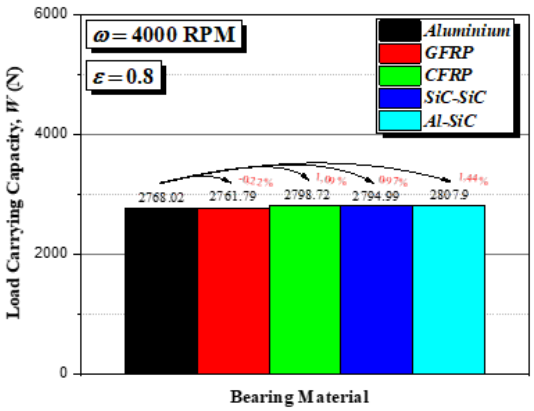

Figure 12: Comparison of the load-carrying capacity of multistep journal bearing at various bearing materials.

Figure 13 shows that the friction force is not significantly affected because of the same condition on the stationary wall, and the largest friction force value is found in Al-SiC and the smallest in aluminum. The graph indicates that variations in materials can impact the magnitude of the resulting friction force. This force is generated by the interaction of the lubricant flow with the shaft walls and bearings. As the lubricant applies more pressure, the frictional force increases. Consequently, changes in material composition directly affect the friction force due to alterations in the deformation of the bearing wall. These material-induced changes affect the rate of momentum in the flowing lubricant, with greater momentum leading to higher friction force values.

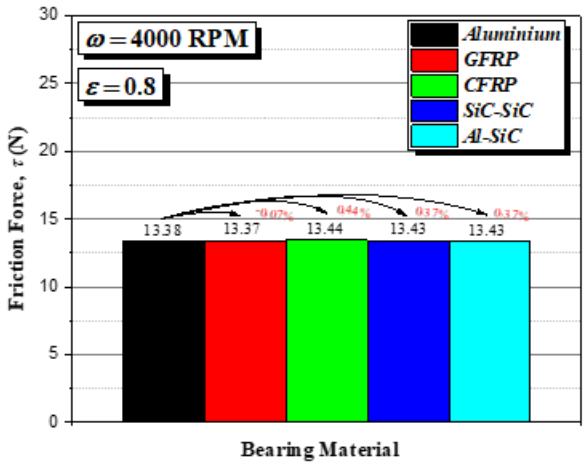

Figure 13: Comparison of the friction force of multistep journal bearing at various bearing materials.

Figure 14 shows that the average acoustic power level is not significantly affected because of the same value of the turbulent intensity in the fluid flow. The largest acoustic power level value is found in *Al-SiC* and the smallest in aluminum. Tribological performance of the elastohydrodynamic lubrication on multistep journal bearing with the change of bearing composite with an eccentricity ratio of 0.8 and rotation speed of 4000 RPM only affects the pressure results, which will affect the value of the load carrying capacity because the modulus value will affect the deformation which will become smaller as the modulus value increases. The friction force value that occurs between the lubricant and the bearing and shaft walls can influence the acoustic level value. Subsequently, the material affects the acoustic level because it provides a value for the friction force.

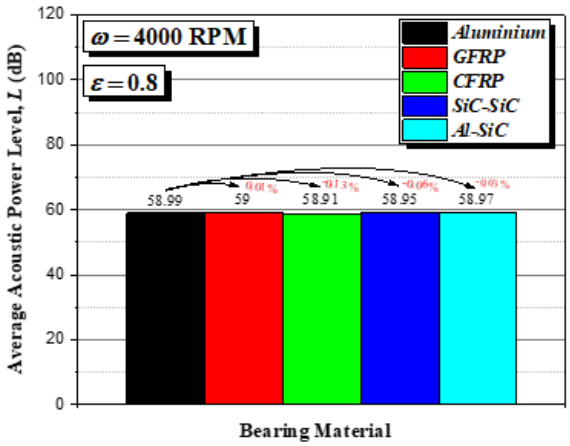

Figure 14: Comparison of the average acoustic power level of multistep journal bearing at various bearing materials.

3.3 Effect of Roughness

In this section, the assessment and comparison of tribological performance of elastohydrodynamic lubrication in multistep journal bearing under various roughness conditions, including smooth (0 µu Ra), precision (0.1 µR Ra), fine (0.4 µR Ra), medium (1.6 µR Ra), and rough (6.3 µR Ra), are conducted while maintaining an eccentricity ratio of 0.8 and a rotation speed of 4000 RPM. R_a is calculated as roughness average of a surface measured microscopic peaks and valleys. This section will discuss tribological performances, which are the load-carrying capacity, frictional force, and average acoustic power level (dB).

Figure 15 shows the decrease in pressure as roughness increases. This phenomenon occurs because surfaces with higher roughness have deformed surface asperities, leading to an increased presence of vapor bubbles in the divergent area. This, in turn, causes more gas bubbles to become trapped in the asperities, resulting in a higher vapor volume fraction within the fluid. Consequently, this lowers the hydrodynamic pressure and peak pressure of the remaining lubricant in the convergence region. This reduces the force acting on the shaft, resulting in a decrease in pressure values, which can affect the load-carrying capacity.

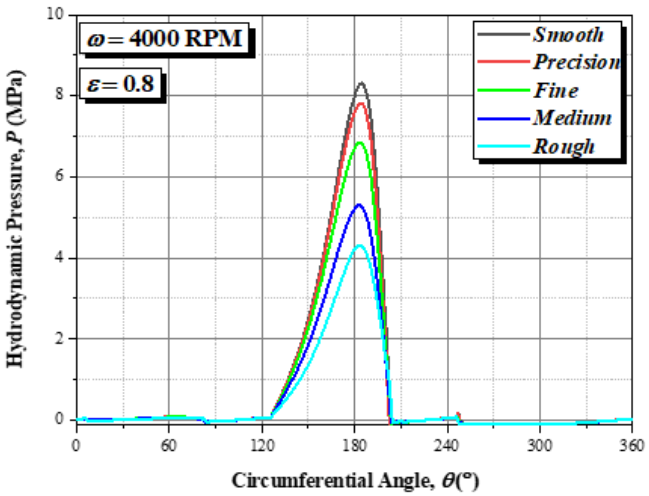

Figure 15: Comparison of the pressure distribution on multistep journal bearing at various roughness levels.

Figure 16 shows that the load-carrying capacity is significantly affected because of the hydrodynamic pressure that declines with increasing roughness levels. The largest load-carrying capacity value is found in the smooth texture and the smallest in the rough texture. This occurs as a result of changes in the value of hydrodynamic pressure in the previous parameter. The higher the hydrodynamic pressure value, the rougher the surface. The lower the hydrodynamic pressure, the lower the load-carrying capacity. These differences in bearing surface conditions directly impact pressure values and load-carrying capacity.

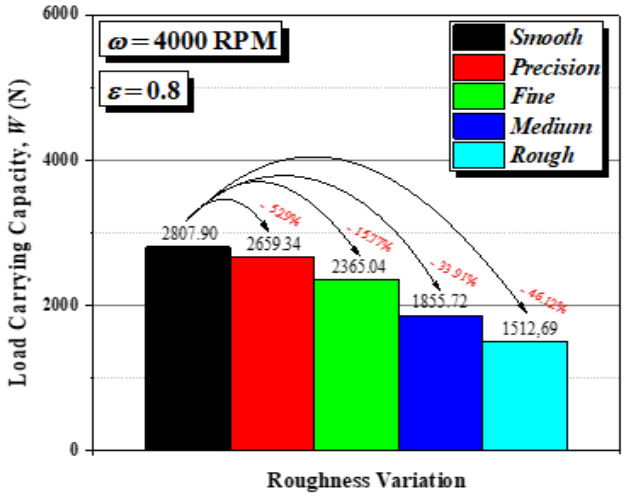

Figure 16: Comparison of the load-carrying capacity of multistep journal bearing at various roughness levels.

Figure 17 shows that the friction is significantly affected because the fluid flow in the stationary wall will be less due to the effect of surface roughness which results in less friction. The smallest friction force value is found in the rough texture and the largest value in the smooth texture. This occurs as a result of changes in pressure values in the preceding parameters. The lower the pressure on the bearing, the greater the surface roughness value. The pressure drop reduces the collision momentum of the fluid particles flowing through the bearing. A reduction in the lubricant impact momentum value results in a reduction in the friction force that occurs in the wall area, resulting in a reduction in the friction force value.

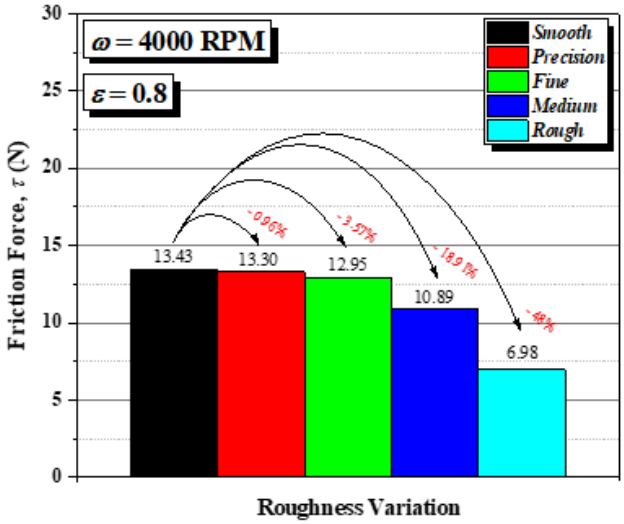

Figure 17: Comparison of the friction force of multistep journal bearing at various roughness levels.

Figure 18 shows that the average acoustic power level is not significantly affected because of the turbulent intensity value in the fluid flow. The largest acoustic power level value is found in the precision texture and the smallest in the rough texture.

The lubrication performance in elastohydrodynamic lubrication for multistep journal bearing is affected by variations in roughness levels, particularly with an eccentricity ratio of 0.8 and a rotation speed of 4000 RPM.

From an engineering perspective, these results indicate that the finishing process for achieving the desired surface roughness levels of contacting surfaces should be properly performed to avoid manufacturing errors and provide the best lubrication performance.

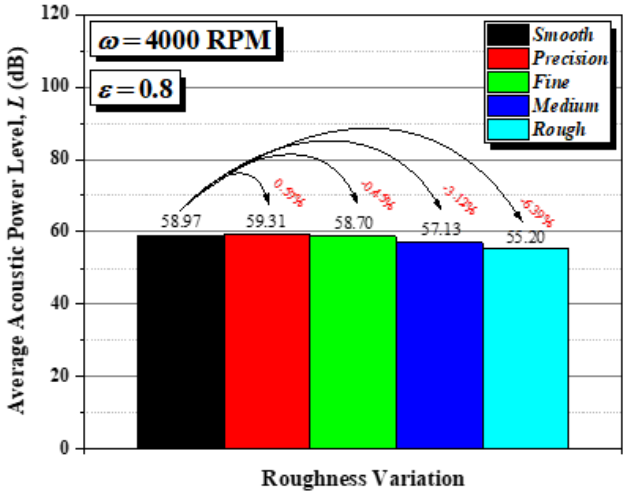

Figure 18: Comparison of the average acoustic power level of multistep journal bearing at various roughness levels.

3.4 Velocity Profile

In this section, the velocity profile introduced by multistep journal bearing lubrication flow will be discussed. Figure 19 shows the velocity vector and contour.

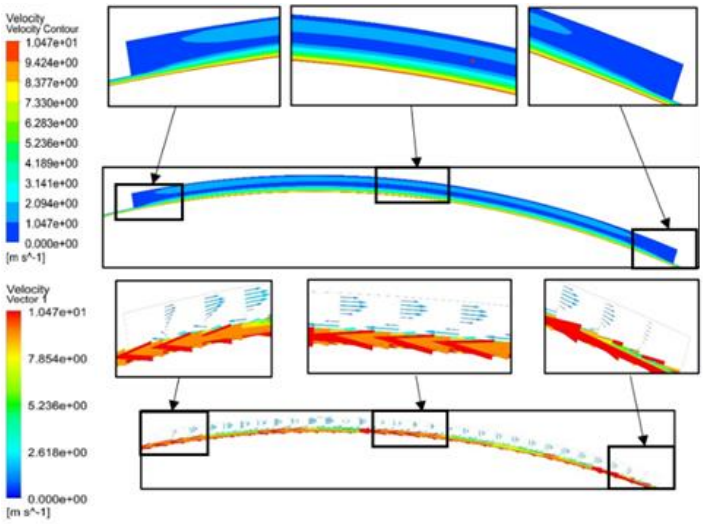

Figure 19: Velocity vector and contour caused by textured multistep journal bearing.

The maximum speed in the simulation closely matches the rotational speed of the moving wall. This arrangement is a consequence of modeling a no-slip condition, where the velocity near the static wall reaches zero. The changes in flow direction near the wall are primarily induced by the flow colliding with the wall perpendicular to the journal rotation.

Backflow refers to the resulting change in flow direction. This phenomenon occurs when the direction of the flow changes, as shown in Figure 19. Different flow velocities in each direction are introduced by the presence of backflow.

CONCLUSIONS

In conclusion, the CFD-FSI method was used to investigate the lubrication capabilities of plain and multistep journal bearing. In this research, it was concluded that increasing the eccentricity ratio did not always increase the load-carrying capacity, tribological performance increased at eccentricity ratios of 0.2 and 0.4 but decreased at 0.6 and 0.8. At an eccentricity ratio of 0.8, increasing roughness led to a decrease in friction force (6.98 N) but was accompanied by a drop in load-carrying capacity (1512.69 N). Additionally, the acoustic power level reached the highest precision roughness of 59.31 dB and had a minimum value for the highest roughness with a value of 55.20 dB. For bearing material, the higher the elastic modulus of the material, the lower the pressure due to deformation, with carbon composite material having the highest pressure value.

NOMENCLATURE

A : Area
B : Arc length between step
C : Clearance
D : Bearing diameter
d : Step depth
E : Elastic modulus
F_f : Friction force
L : Bearing length
L_p : Acoustic power level
p : Pressure
R_a : Roughness average
R_b : Bearing radius
R_j : Journal radius
ν : Poisson ratio
W : Load carrying capacity
γ : Arc length step
ε : Eccentricity ratio
μ : Viscosity
ρ : Density
τ : Wall shear
Φ : Volume fraction
$\emptyset$: Orientation angle
ω : Rotational speed

ACKNOWLEDGMENTS

This research is fully supported by RPI (Research Publication International) grant, No. 569-135/UN7.D2/PP/IV/2023. The authors fully acknowledged the Institute for Research and Community Services (LPPM), Universitas Diponegoro for the approved fund which makes this important research viable and effective.

REFERENCES

Adams, T., Grant, C., & Watson, H. (2012). A simple algorithm to relate measured surface roughness to equivalent sand-grain roughness. International Journal of Mechanical Engineering and Mechatronics, 1(2), 66-71.

Bompos, D. A., & Nikolakopoulos, P. G. (2016). Tribological design of a multistep journal bearing. Simulation Modelling Practice and Theory, 68, 18-32.

Chen, Y., Feng, J., Sun, Y., Peng, X., Dai, Q., & Yu, C. (2020). Effect of groove shape on the hydrodynamic lubrication of journal bearing considering cavitation. Engineering Computation, (Swansea, Wales), vol. 37, no. 5, 1557–1576.

Cupillard, S., Cervantes, M. J., & Glavatskih, S. (2008). A cfd study of a finite textured journal bearing. IAHR 24th Symposium on Hydraulic Machinery and Systems.

Dhande, D. Y., & Pande, D. W. (2017). A two-way FSI analysis of multiphase flow in hydrodynamic journal bearing with cavitation. Journal of the Brazilian Society of Mechanical Sciences and Engineering, 39(9), 3399-3412.

Groover, M.P. (2013). Fundamentals of Modern Manufacturing: Materials, Processes, and Systems, 5th Edition. Wiley.

Javorova, J., Stanulov, K., Alexandrov, A., & , Iliuta, V. (2016). Journal bearings lubrication of non-newtonian lubricants with surface roughness effects. Journal of the Balkan Tribological Association, vol. 22, no. 1, 433–443.

Lahmar, M., Ellagoune, S., & Bou-Saïd, B. (2010). Elastohydrodynamic lubrication analysis of a compliant journal bearing considering static and dynamic deformations of the bearing liner. Tribology Transactions, 53(3), 349-368.

Liang, X., Liu, Z., Wang, H., Zhou, X., & Zhou, X. (2016). Hydrodynamic lubrication of partial textured sliding journal bearing based on three-dimensional CFD. Industrial Lubrication and Tribology, vol. 68, no. 1, pp. 106–115.

Meng, F., Wei, Z., Minggang, D., & Gao, G. (2016). Study of acoustic performance of textured journal bearing. Proceedings of the Institution of Mechanical Engineers, Part J: Journal of Engineering Tribology, 230(2), 156-169.

Muchammad, Tauviqirrahman, M., Soetopo, H. S. S., & Jamari. (2021). Mechanical and thermal deformations effects on plain journal bearing with isoviscous boundary condition based on CFD and FSI methods. Jurnal Tribologi, 28, 63-81.

Muchammad, M., Tauviqirrahman, M., Mario, L. & Jamari, J. (2022a). Thermo-hydrodynamic analysis of multistep texture effect on the performance of journal bearings through acoustic and tribological characteristics. Journal of the Brazilian Society of Mechanical Sciences and Engineering, 44(7), 1-13.

Muchammad, M., Putra, W. D.D. Tauviqirrahman, M. Setiyana, B. Yohana, E. & Jamari, J. (2022b). Investigation of the influence of turbulence to tribological performance on smooth and multistep journal bearing with hydrodynamics simulation. Frontiers in Mechanical Engineering, 8, 1-12.

Lin, Q., Bao, Q., Li, K., Khonsari, M. M., & Zhao, H. (2018). An investigation into the transient behavior of journal bearing with surface texture based on fluid-structure interaction approach. Tribology international, 118, 246-255.

Sander, D. E., Allmaier, H., Priebsch, H. H., Witt, M., & Skiadas, A. (2016). Simulation of journal bearing friction in severe mixed lubrication–Validation and effect of surface smoothing due to running-in. Tribology international, 96, 173-183.

Singh, N., & Awasthi, R. K. (2020). Theoretical investigation of surface texture effects on the performance characteristics of hydrodynamic two-lobe journal bearing. Proceedings of the Institution of Mechanical Engineers, Part J: Journal of Engineering Tribology, 234(11), 1712-1725.

Song, Y., Gu, C. W., & Ren, X. (2015). Development and validation of a gaseous cavitation model for hydrodynamic lubrication. Proceedings of the Institution of Mechanical Engineers, Part J: Journal of Engineering Tribology, 229(10), 1227-1238.

Tala-Ighil, N., Fillon, M. & Maspeyrot, P. (2011). Effect of textured area on the performances of a hydrodynamic journal bearing. Tribology International, vol. 44, no. 3, 211–219.

Tauviqirrahman, M., Jamari, J., Wibowo, B. S., Fauzan, H. M. & Muchammad, M. (2019). Multiphase computational fluid dynamics analysis of hydrodynamic journal bearing under the combined influence of texture and slip. Lubricants, vol. 7, no. 11, 1-31.